Geomorphic implications of gravity currents created by changing initial conditions

Zordan Jessica[1], Schleiss Anton J.[1], and Franca Mário J.[1,2]

[1]Laboratory of hydraulic constructions (LCH), School of Architecture, Civil and Environmental Engineering, École Polytechnique Fédérale de Lausanne (EPFL), 1015 Lausanne, Switzerland
[2]River Basin Development chair group, Water Science and Engineering department, IHE Delft Institute for Water Education, 2611 Delft, The Netherlands

Correspondence to: Zordan Jessica (jessica.zordan@epfl.ch)

Abstract. Gravity currents reproduced in laboratory by the lock-exchange technique are here tested for three initial densities and five lock-lengths, for horizontal and four inclinations of the lock. The main purpose is to quantify the effect of the increment of gravitational forces, due to the introduction of a slope, on the hydrodynamics of gravity currents and consequently on its transport capacity. The shape of the current is altered due to the enhanced entrainment of ambient water and mainly the body

5 of the current results affected. A range of slopes is tested, going from horizontal to a limit case in which two mechanisms compete, i.e. the current entrainment of water from the upper surface due to the increment of friction and the head feeding by the rear steady current. In particular, bed shear stress and the corresponding geomorphic potential are analysed. Using a base experience where erosion of a mobile bed was investigated, the implications of an inclined lock in the entrainment capacity of the flow is here discussed.

10 ## 1 Introduction

Spontaneous in nature or originated by human activities, many are the occurrences of gravity currents. These flows are created by differences in hydrostatic pressures at the surface of contact of two fluids with density differences. In the atmosphere, examples of gravity currents are katabatic winds or sea breeze fronts, in which the density gradient is caused by temperature inhomogeneities. Avalanches of airborne snow, plumes of pyroclasts from volcanic eruptions and sand storms are atmospheric

15 flows where suspended particles play a major role in producing the density gradient. If suspended sediment confer the extra density, gravity currents take the name of turbidity currents. Turbidity currents are given special attention in what concern reservoirs sedimentation, which have important economical costs due to the loss of volume for water storage (Palmieri et al. (2001), Schleiss et al. (2016)). Among gravity currents caused by human actions, the release of pollutants into rivers, oil spillage in the ocean and the desalination plants outflows are of primary importance due to their negative environmental impacts.

20 Gravity currents have been subjects of research over the last decades. Simpson (1997), Kneller and Buckee (2000), Huppert (2006) and Ungarish (2009) present a comprehensive review of the early work on natural and experimentally reproduced gravity currents. Authors agree on describing the shape of the gravity current as composed by an arising highly turbulent front, called head, followed by, in same cases, a body and a tail. Particularly in the body, that can reach a quasi-steady state, a

vertical structure can be distinguished. A gravity current presents two main interfaces where exchanges concur: at the bottom, generally a solid boundary, and at the top, at the interface with the ambient fluid. These are active boundaries where mass and momentum exchanges are promoted (Ancey, 2012). Ambient fluid is entrained due to shear and buoyancy instabilities at the upper interface (Cantero et al., 2008) resulting in the dilution of the underlying current and modification of the density profile

5 which characterizes a gravity current under stable density stratification (Turner, 1973). If the gravity current travels above an erodible bed, entrainment of material from the bottom can take place, which is conveyed with the current and redeposited sometimes at large distances from their original position. High shear stress associated with intense ejection and burst events influence erosion and bed load transport (Ninto and Garcia (1996), Cantero et al. (2008), Zordan et al. (under review, a)). For example, in the shallow shelf region of the lake it is frequently observed that cold water, relatively denser than that in open

10 waters, starts to descend down the slope as a cold gravity current (Fer et al., 2002). The plume is able to transport suspended sediment together with their dissolved components, oxygen, and pollutants into deeper water.

It is therefore evident that gravity currents can originate under different conditions: changes of initial volume of denser fluid and of the inclination of the bottom represent some of the various configurations that can be found in reality. Thus, to understand how the initial trigger conditions of gravity currents are linked with their transport capacity is of fundamental importance.

15 Gravity currents are here reproduced in laboratory by the lock-exchange technique. Three initial densities are tested in combination with five lock-lengths on horizontal bottom and others four inclinations of the lock. The main purpose is to investigate how the increment of gravitational forces, due to the introduction of a slope in the lock, affect the hydrodynamic of gravity currents and consequently its transport capacity. The tested range of lock-slopes below 8% ($0° \leq \alpha < 5°$) received relatively little attention in previous studies of gravity current down an inclined. Britter and Linden (1980) found a critical

20 angle, which is typically less than a degree, over which buoyancy force is large enough to counter-act the bottom friction producing a steady flow. At larger slopes, two mechanisms affect the evolution of the current: the current entrains water from the upper surface due to the increment of friction and the head is fed by the rear steady current. By testing a range of slopes going from horizontal to a limit case in which these two mentioned mechanisms take place, the transition from a friction governed flow to a flow in which gravitational forces become more and more important is studied.

25 The present paper is structured as such: first the experimental set-up and the process which allows for the noise reduction of the velocity measurements are described. Then, the results are presented: a method for the identification of the shape of the current is here defined and, by means of the mean streamwise velocity field, both bottom and interface shear stresses are computed. The variation on the shape caused by changing initial conditions (i.e. with different initial buoyancies, various lock-lengths and lock-bottom inclinations) are therefore discussed. The potential water entrainment and bottom erosion capacity are

30 estimated on the base of the computed shear stresses evolutions. Finally, an overview of the main findings is presented in the conclusions.

2 Methodology

2.1 Experimental set-up

The tests are performed in a channel with a rectangular section, 7.5 m long and 0.275 m wide. The gravity currents are reproduced through the lock-exchange technique by sudden release of a gate which divides the flume in two parts where the

5   fluids of different densities are at rest. Three buoyancy differences are tested in combination with five lock-slopes, ranging from $S = 0\%$ (horizontal bed) to $S = 8\%$ (tests S0 to S4). Figure 1 shows the configurations from horizontal bed (S0) to the steepest slope (S4). By introducing a slope on the channel lock reach, the volume of denser fluid is reduced. This lock contraction is also tested separately by performing reference tests with the combination of the three initial densities and the five lock-lengths which correspond to the volumes in the lock of the tests under inclined. The experimental parameters are reported in Table 1.

10   $R_i.S_i$ refer to gravity currents reproduced by different initial density with the presence of a lock-slope while $R_i.L_i$ indicates the tests with varying initial density and lock-length.

    The channel is filled with 0.2 m of ambient water in one side and of salty water, up to the same level, in the lock reach. Once the gate is removed, the saline current forms. At 2.5 m from the gate an Acoustic Doppler Velocity Profiler (ADVP) is placed to measure 3D instantaneous velocities along a vertical. The ADVP (Lemmin and Rolland (1997), Hurther and Lemmin (2001),

15   Franca and Lemmin (2006)) is a non-intrusive sonar instrument that measures the instantaneous velocity profiles using the Doppler effect without the need of calibration and was used with an acquisition frequency of 31.25 Hz. The velocity profiles are collected in time along a fixed vertical. The flume is connected to a final big reservoir that allows the current dissipation and avoids its reflection upstream.

    Normalization of the time is made using the scale $t^* = h_b/u_b$, where h_b is a vertical geometric scale, here considered as one

20   third of the total height of the fluid in the experimental tank, h_0 ($h_b = h_0/3$ and $h_0 = 0.2$ m) and $u_b = \sqrt{g'h_b}$ is the buoyancy velocity.

2.2 Data filtering

By means of the analysis of the power spectra of the raw data collected with the ADVP, noisy frequencies were mainly detected below 8 Hz. The instantaneous measurements were thus low-pass filtered with 8 Hz as cut-off frequency. The time-

25   series of the mean streamwise and vertical velocities ($\overline{u}$ and $\overline{w}$) for the unsteady gravity current, were derived after a filtering procedure that consisted in the application of a moving average over a time-window which is chosen by the analysis of the power spectra distribution as in Baas et al. (2005). This analysis showed that for a time window of 0.32 s, the harmonics of all the meaningful frequencies were still recognisable while, increasing the time window, the harmonics of progressively smaller frequency gradually lose power and they become impossible to distinguish (Baas et al., 2005). Thus, this window length was

30   chosen for the moving average defining $\overline{u}$ and $\overline{w}$. The turbulent fluctuation time series (u' and w') is then calculated using the Reynolds decomposition:

$$u = \overline{u} + u' \tag{1}$$

S_i tests	ρ_0 $\left[\frac{kg}{m^3}\right]$	g'_0 $\left[\frac{m^2}{s}\right]$	u_0 $\left[\frac{m}{s}\right]$	Re_0 $[-]$	S $[\%]$	α $[°]$	V_i/V_0
R1.S0	1028	0.29	0.24	48166	0	0.00	1.000
R1.S1	1028	0.29	0.24	48166	2	1.15	0.750
R1.S2	1028	0.29	0.24	48166	4	2.29	0.625
R1.S3	1028	0.29	0.24	48166	6	3.43	0.500
R1.S4	1028	0.29	0.24	48166	8	4.57	0.250
R2.S0	1038	0.39	0.28	55857	0	0.00	1.000
R2.S1	1038	0.39	0.28	55857	2	1.15	0.750
R2.S2	1038	0.39	0.28	55857	4	2.29	0.625
R2.S3	1038	0.39	0.28	55857	6	3.43	0.500
R2.S4	1038	0.39	0.28	55857	8	4.57	0.250
R3.S0	1048	0.49	0.31	62610	0	0.00	1.000
R3.S1	1048	0.49	0.31	62610	2	1.15	0.750
R3.S2	1048	0.49	0.31	62610	4	2.29	0.625
R3.S3	1048	0.49	0.31	62610	6	3.43	0.500
R3.S4	1048	0.49	0.31	62610	8	4.57	0.250

L_i tests	ρ_0 $\left[\frac{kg}{m^3}\right]$	g'_0 $\left[\frac{m^2}{s}\right]$	u_0 $\left[\frac{m}{s}\right]$	Re_0 $[-]$	L_i $[m]$	V_i/V_0 $[-]$
R1.L0	1028	0.29	0.24	48166	2.500	1.000
R1.L1	1028	0.29	0.24	48166	1.875	0.750
R1.L2	1028	0.29	0.24	48166	1.563	0.625
R1.L3	1028	0.29	0.24	48166	1.250	0.500
R1.L4	1028	0.29	0.24	48166	0.625	0.250
R2.L0	1038	0.39	0.28	55857	2.500	1.000
R2.L1	1038	0.39	0.28	55857	1.875	0.750
R2.L2	1038	0.39	0.28	55857	1.563	0.625
R2.L3	1038	0.39	0.28	55857	1.250	0.500
R2.L4	1038	0.39	0.28	55857	0.625	0.250
R3.L0	1048	0.49	0.31	62610	2.500	1.000
R3.L1	1048	0.49	0.31	62610	1.875	0.750
R3.L2	1048	0.49	0.31	62610	1.563	0.625
R3.L3	1048	0.49	0.31	62610	1.250	0.500
R3.L4	1048	0.49	0.31	62610	0.625	0.250

Table 1. Experimental parameters. ρ_0 is the initial density of the mixture in the upstream tank (measured with a densimeter), g' is the reduced gravity corresponding to ρ_0, $Re_0 = u_0 h_0 / \nu_c$ is the Reynolds number based on initial quantities with $u_0 = \sqrt{g' h_0}$ the initial buoyancy velocity, $h_0 = 0.2$ m the total height of the water column and ν_c the kinematic viscosity of the denser fluid, α is the angle of inclination of the bottom in the lock, S is the lock-slope expressed in percentage (h_{S_i}/L_0, with h_{S_i} the height as in Figure 1), L_i is the length of the upstream lock-reach, V_i/V_0 the percentage of volume of the upstream lock-reach with respect to the configuration L_0, and ΔT is the difference in temperature between the temperature of the mixture, T_0, and the temperature of the ambient water, T_a (measured with a thermometer before each experiment).
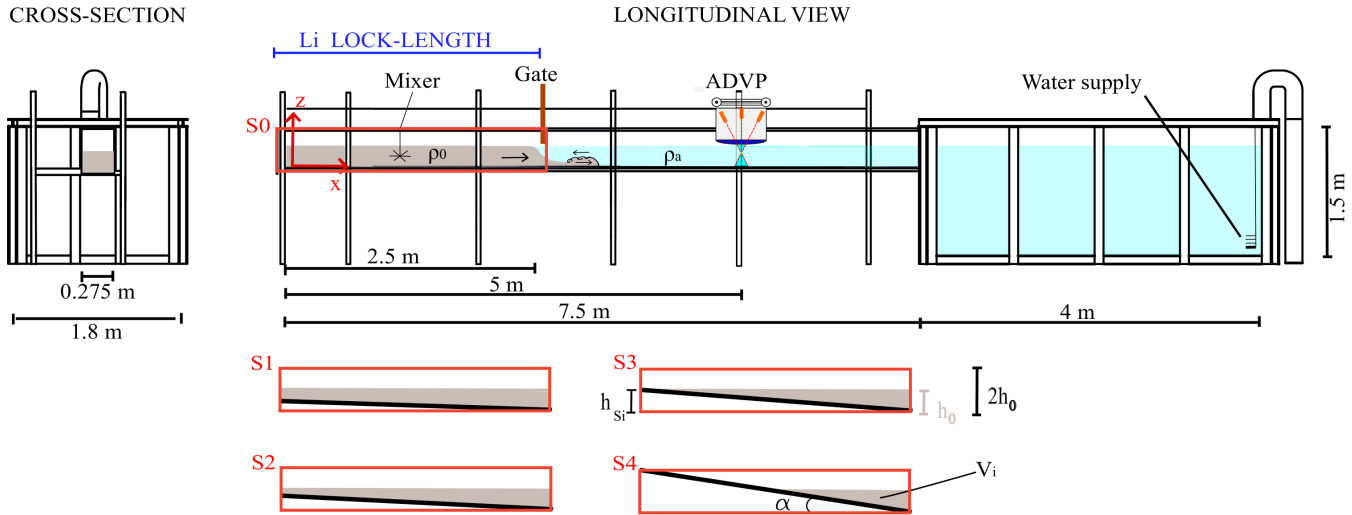
Figure 1. Longitudinal view and cross-section of the experimental set-up showing tested slope configurations S0 to S4 of lock volumes V_i.

where u is the instantaneous velocity. The cleaning procedure with the velocity signals and corresponding spectra is shown in Figure 2.

3   Results

3.1   The shape of the current

5   A definition that allow to distinguish the head and the body regions of the current is considered in order to analyse the current shape changes due to the presence of the slope in the lock. In particular, a criterion is here established to identify the two main regions of a gravity current: the head and the body. A kinematic function (H) is defined and computed as the product between the instantaneous depth averaged streamwise velocity, $u_d(t)$:

$$u_d(t) = \frac{1}{h} \int_0^h u(z,t)dz \tag{2}$$

10   and the current height, $h(t)$, that is here identified by the position where the streamwise velocity is equal to zero, as in Zordan et al. (under review, a). H is thus defined as:

$$H(t) = u_d(t)h(t) \tag{3}$$
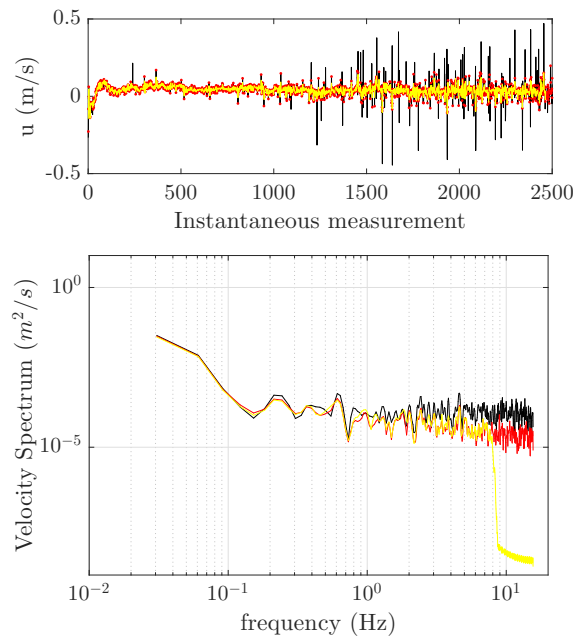
Figure 2. Raw velocity data (black) and despiked data (red) obtained with the procedure proposed by Goring and Nikora (2002). Then, through the analysis of the velocity spectra (figure at the bottom), the cut-off frequency of 8 Hz has been identified in order to low pass filter the noisy frequencies (yellow line).

As in Nogueira et al. (2014), where a similar procedure was adopted considering the product of the depth averaged streamwise velocity by the depth averaged density of the current, the downstream limit of the head (L_h) is identified by the first meaningful local minimum of the function H, starting from the front.

The body length is instead analysed by using the cumulative sum of the function H. This is a region where a quasi-steady regime is established for a certain time length. This implies that $\sum H$ shows a linear increment in time. The limit of the body is therefore here defined by analysing the linear evolution that is fitted by a linear regression with least squares method for progressively longer portion of the accumulated summed data. The analysis of the development of R^2 value allows to find the extension of the linear portion which corresponds to the temporal extent of the body region (L_b). In Figure 3 the development of the function H is shown for the tests with the lock-slope.

The same procedure is adopted for tests $R_i.L_i$ and the results can be find in Zordan et al. (under review, b).

The form of the currents was identified by the zero streamwise velocity contour. In Figure 4 the contours of each test with the lock-slope are compared with the correspondent reference test with lock-length variation. The results are grouped by the initial density on the lock (columns in the figure), and by pairs of tests with the same volume of the lock but for different slopes. The extension of head and body as identified by the previous methods are also reported with the vertical lines. Dashed lines refers to tests S_i while continuous lines correspond to L_i tests.
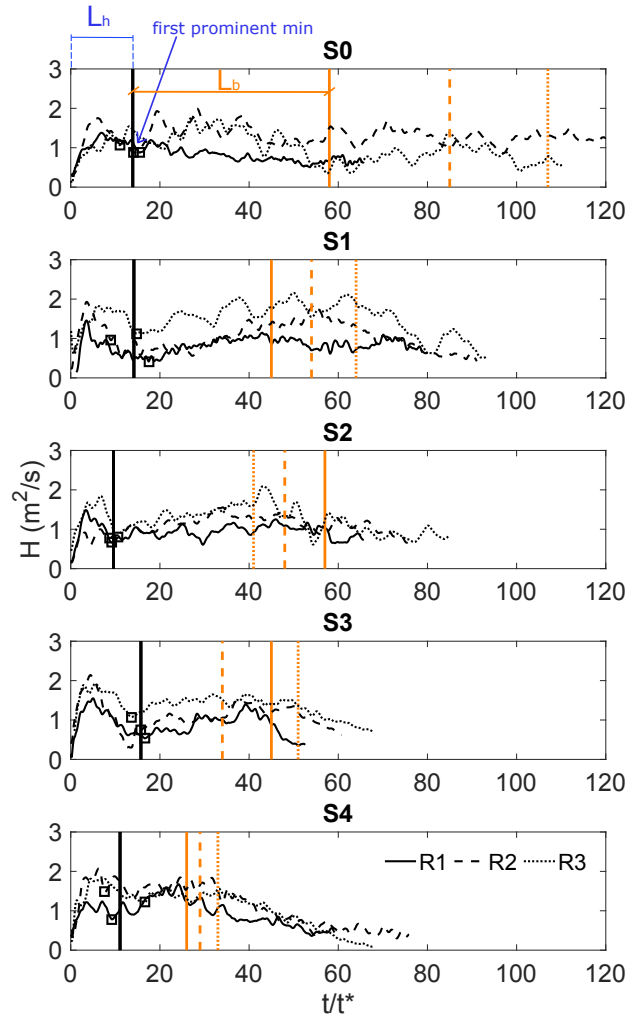
Figure 3. Determination of the gravity current head extension from the first prominent minimum of the function H (L_h). The extension of the body (L_b), as identified by the cumulative sum of the depth-averaged streamwise velocity, is also traced with the red vertical lines.

In Figure 4 we can see that the head of the current does not show any relevant change. Instead the extension of the body is affected: it reduces with increasing inclination of the bed and the same goes for tests produced by reduced lock volume. A dependency on the initial density is noticed and in three out of the total five slopes bring to the formation of longer body with greater initial buoyancy. This can be verified in Figure 3 where extensions of the bodies are traced with the vertical orange
5 lines. R1, R2 and R3 produces progressively longer bodies for tests S0, S1 and S4.

The largest deviation between the two contours of corresponding tests L_i - S_i is noticed for the last configuration, with the R_i.L4 tests showing a shorter body and a more defined tail while for the correspondent tests with the inclined lock the body is more extended.
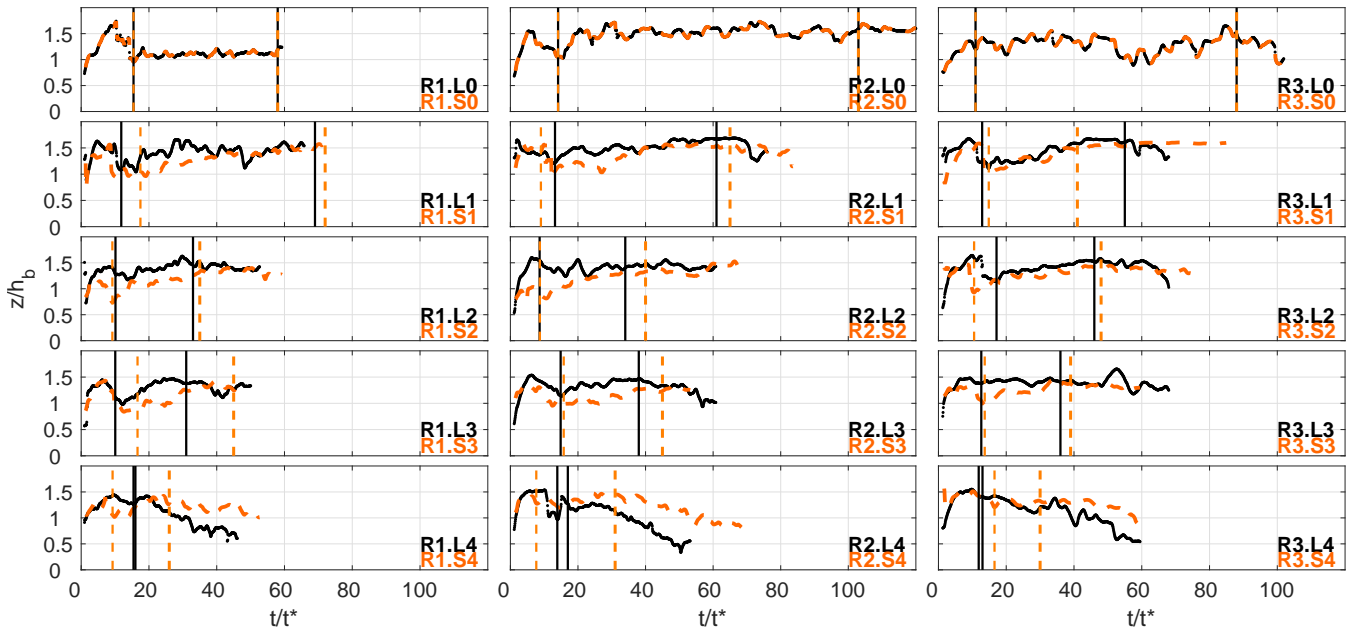
Figure 4. Gravity currents contours, as identified by the zero streamwise velocity contour, for tests with the lock-slope and correspondent tests with lock-length variation.

3.2 Mean velocity field

In Figure 5 the mean streamwise velocity field on the background and velocity vectors of the components $(\overline{u}, \overline{w})$ are shown for all the tests performed. The heads of the currents are indicated by the vertical dashed lines and the zero streamwise velocity contours are marked by the black lines. We can notice that the structures of the currents are quite similar in all configurations.

5   An arising head is followed by a zone of high mixing, characterized by the presence of billows (due to Kelvin-Helmholtz type of instabilities (Simpson, 1972)) that are due to shear at the rear part of the elevated head. Body and tail are not always well defined regions, mainly for the class of tests down an inclined, and therefore the contour is not drawn. Moreover, tests S_i show lower streamwise velocities within head and body with respect to correspondent L_i tests.

    Mean streamwise velocity is slightly higher for tests on horizontal bed. This can appear to some extent contradictory but that

10 behaviour has already been mentioned in literature, in the study of Beghin et al. (1981), who was one of the first to investigate the role of the slope on the physics of a gravity current. He showed that tests which flows on small slopes (typically less than 5° as it is the case here) experience a first acceleration phase followed by a deceleration phase. This is because of the fact that, although the gravitational force increases as the lock-slope becomes more vertical, there is also increased entrainment, both into the head itself and into the flow behind. This produces an extra dilution of the current with a decrease in buoyancy.
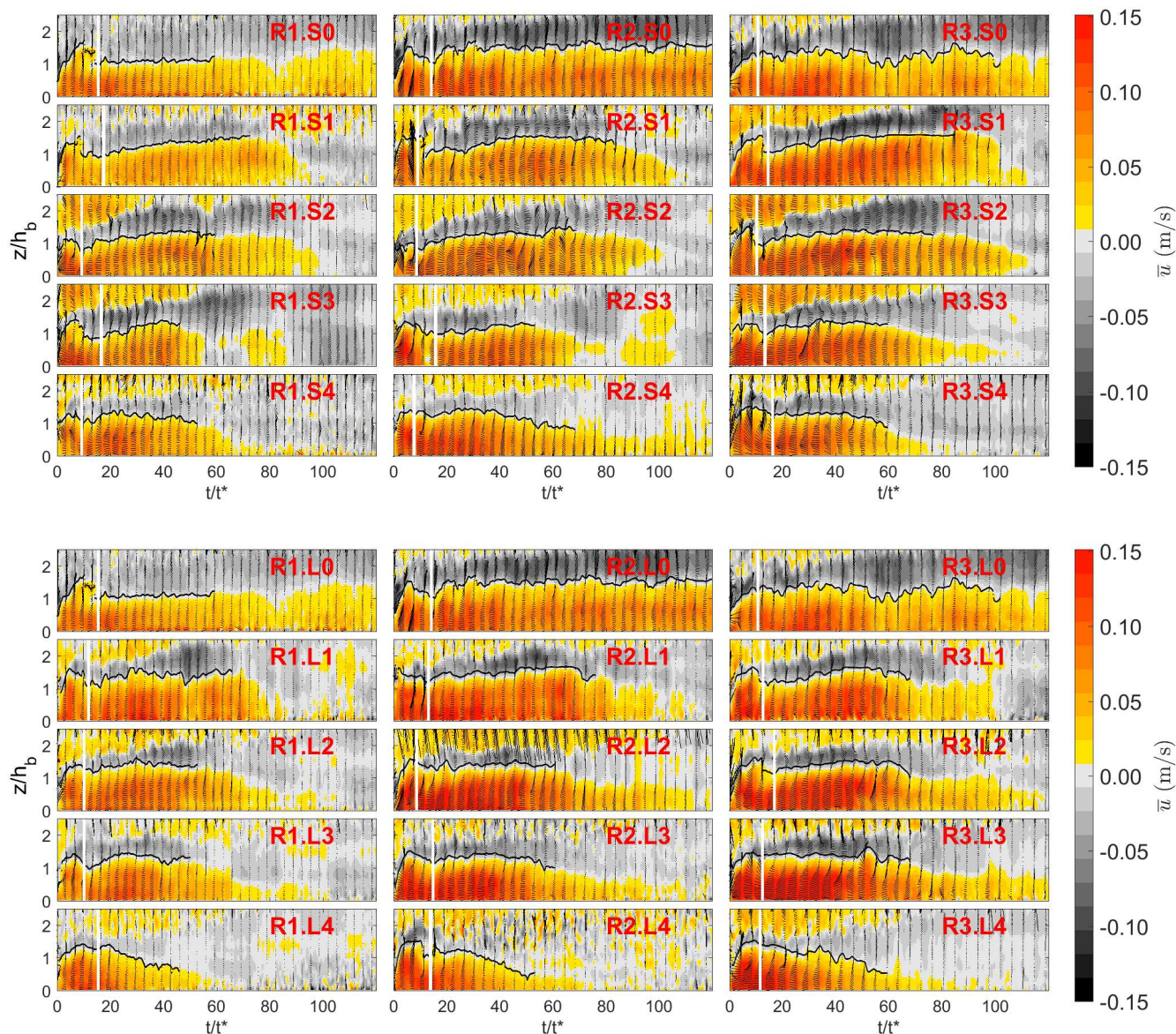
Figure 5. Streamwise velocity field on the background and velocity vectors of the components (u,w). The head of the current is delimited by the vertical white line. The contour of the current is indicated in black.

3.3 Bottom and upper shear stress

The sedimentological impact of a gravity current is the result of the complex hydrodynamic of this flow. Sediment entrainment is a complex mechanism mainly due to the difficulty in defining the fluctuating nature of turbulent flow (Salim et al., 2017).

Earth Surf. Dynam. Discuss., https://doi.org/10.5194/esurf-2017-63

In Zordan et al. (under review, a) the transport of sediment within a gravity current is linked to the bed shear stress, that is here considered a "surrogate" measure of it. The form that bed shear stress is affected by the changing initial conditions of the current explains thus how the entrainment capacity of a current is altered. Bed shear stress temporal evolution is calculated by following the procedure in Zordan et al. (under review, a). Under the assumption of flow gradually varied in the longitudinal

5   direction, essentially two dimensional in vertical plane, and with high relative submersion, the longitudinal velocity in the overlapping layer can be fitted by the logarithmic law of the wall as (Ferreira et al., 2012):

$$\frac{\overline{u}(z)}{u_*} = \frac{1}{k} \ln \frac{z}{z_0} \tag{4}$$

where $\overline{u}(z)$ is the mean velocity, u_* is the friction velocity, which is the velocity scale corresponding to the bed shear stress (Chassaing, 2010), k is the von Kármán constant, z is the vertical coordinate and z_0 is the zero-velocity level. Here the flow

10   boundary is assumed to be smooth and the classic value of the von Kármán constant of $k = 0.405$ is adopted. Discussion on the estimation of k can be found in Ferreira (2015).

The fitting of the logarithmic law of the wall is used to calculate the friction velocity and bed shear stress is afterwards computed by considering a constant initial density that is here equal to the initial density in the lock(ρ_c):

$$\tau_b = \rho_c u_*^2 \tag{5}$$

15   The fitting procedure of the bottom logarithmic layer was determined stepwise, extending a linear least square fitting range (in a semi-logarithmic scale) from the lowest measured point until the maximum velocity vertical position. The layer providing the best regression coefficient was chosen and considered for the estimation of u_*, corresponding to the extent of the logarithmic layer.

The bed shear stress time-evolution of gravity currents with lock-slope ($\tau_{b,S}$) are compared to the analogous results for tests

20   with decreasing lock ($\tau_{b,L}$) (Figure 6). Tests performed on an inclined bottom show in average lower values of bed shear stress with the only exception of tests S4, which is the steepest slope condition, where, from normalized time $t/t^* \simeq 20$, i.e. in the body region, bed shear stress is slightly higher than in the correspondent L$_i$ tests.

At the upper boundary of the gravity currents, i.e. the interface with the ambient water, studies on turbulent flow near a density interface confirmed that under certain conditions, the turbulent boundary layer theory can be applied as well (Lofquist

25   (1960), Csanady (1978)) and that the "law of the wall" can be applied to estimate the shear stress here. By hypothesizing a constant mean value of water viscosity and hydraulically smooth conditions, the estimation of an interface shear stress (τ_m) is made; qualitatively the estimation that will result is enough for the purpose of the present study. The time evolution of interface shear stress is therefore computed following the same procedure as for the bottom shear stress. In this case the fitting procedure of the logarithmic layer is determined by considering the mixing layer as defined in (Zordan et al., under review, b). This layer

30   is delimited at the top by the zero streamwise velocity contour and at the bottom by the height of the current as defined by the Turner's integral scales (Ellison and Turner, 1959). Within this layer the at-least-three consecutive measurement points along the velocity profile which were giving the highest R^2 were considered for fitting. The time evolution of interface shear stress for the two series of tests is shown in Figure 7. Again the main differences between tests with reduced lock and respective tests
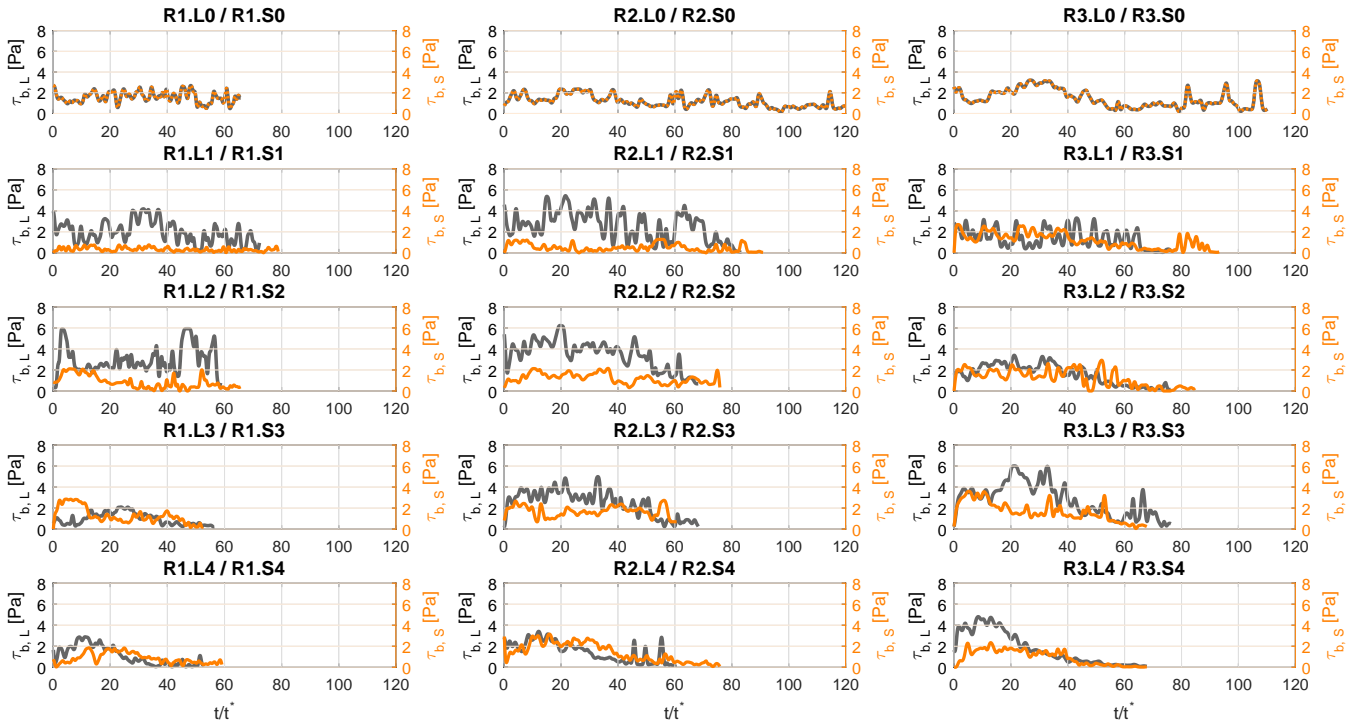
Figure 6. Temporal evolution of bed shear stresses calculated by log law fitting for tests with progressively reduced lock-length ($\tau_{b,L}$) and with the lock-slope ($\tau_{b,S}$).

with lock-slope are for the fourth configuration: the steepest slopes present higher values of interface shear stress in the body region with respect to the correspondent tests with the same initial volume of release but flowing on a horizontal bed.

4 Discussion

4.1 Shape variation of gravity current with the lock-slope

5   The extensions of the body of correspondent tests performed with the lock-slope or on horizontal bed with varying lock-lengths are compared in Figure 8. For lower slopes the body extension is similar to the currents produced with the same lock-volume but with horizontal bottom. However, for slopes higher than 6%, the body region for tests S_i are longer than correspondent tests L_i. This behaviour agrees with the study of Britter and Linden (1980) where they indicated that a critical angle exists over which buoyancy force is large enough to counteract the bottom friction and produce a steady flow. This critical bed slope

10   was find to be of around 1.8% (which corresponds to a bottom inclination of $\approx 1°$). At this point two mechanisms affect the evolution of the current: the current entrains water from the upper surface due to the increment of friction and the head is fed by the rear steady current. The flow of tests $S4$ show these characteristics: (i) an extended body is the result of water entrainment at
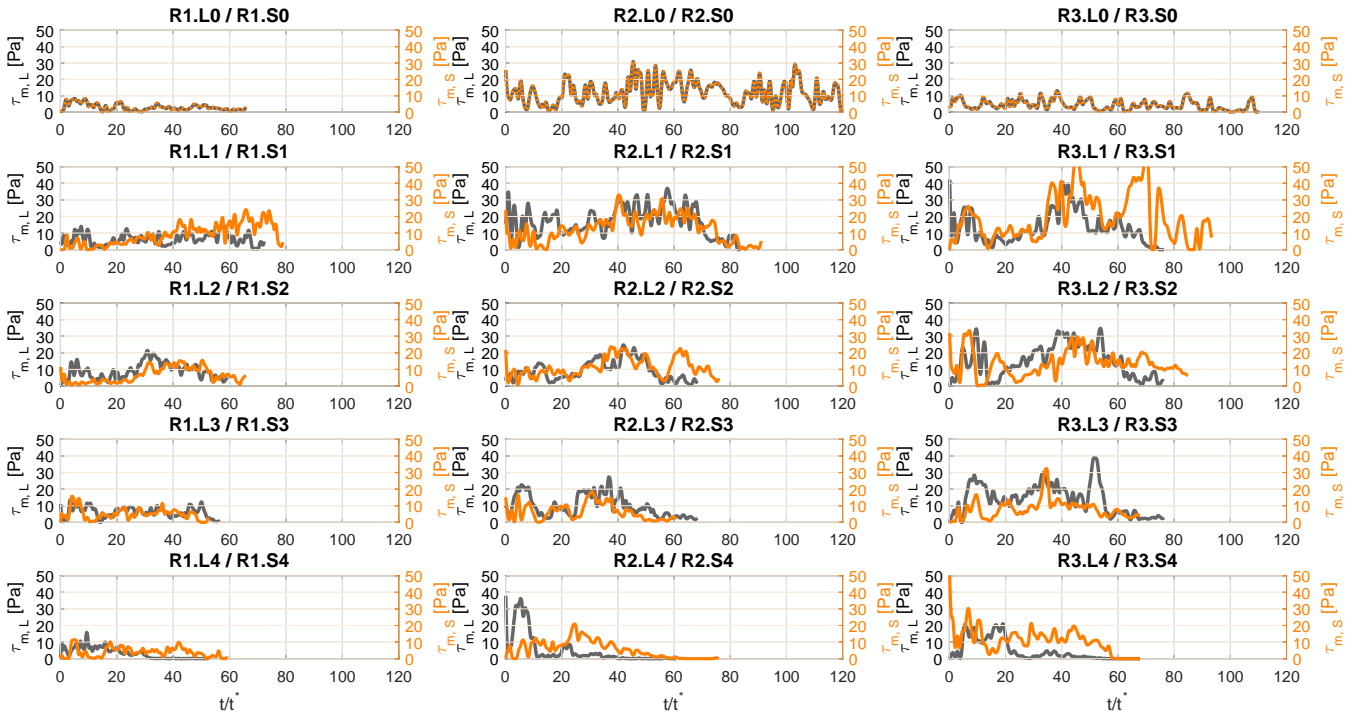
Figure 7. Temporal evolution of interfacial shear stresses calculated by log law fitting for tests with progressively reduced lock-length ($\tau_{m,L}$) and with the lock-slope ($\tau_{m,S}$).

the upper surface of the current that creates dilution and expansion of the fluid in the current; (ii) the fluid in the body become faster as a result of the gravitation forces as in Britter and Linden (1980) (Figure 5). Britter and Linden (1980) showed that, while with currents flowing along a horizontal boundary, the head is the controlling feature, down a slope, the body becomes more determinant in the gravity current evolution since it is up to 30-40% faster than the head velocity, depending on the slope,

5   being able therefore to move faster material into the head. In our study this is verified only for lock-slopes larger than 6%.

4.2 Ambient entrainment

A new quantity is defined which account for the potential entrainment capacity of the gravity current on the base of the computed time evolution of the interfacial shear stress (τ_m). It is computed as the non-dimensional time integral of the shear stress which represents, after dimensional analysis, the work done over a determined duration, per unit surface for a given

10   advection velocity, being the initial buoyancy velocity, u_0, a proxy of this latter. This quantity Φ_m is calculated as:

$$\Phi_m = \int_{T_1}^{T_2} \tau_m(t) dt / t^* \tag{6}$$
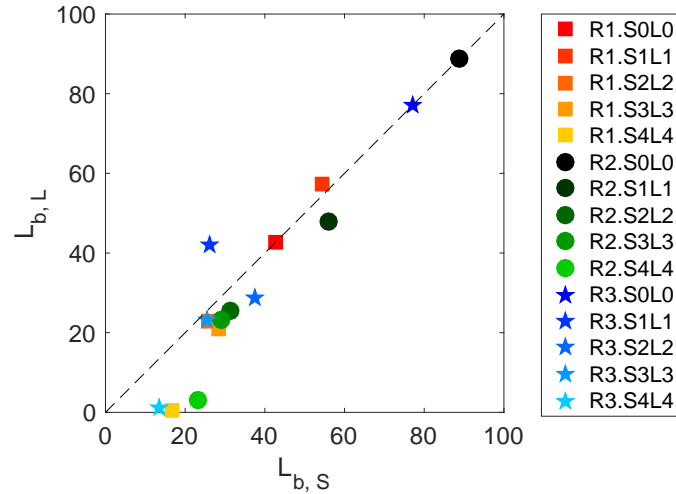
Figure 8. Comparison of the length of the body (L_b) between tests with progressively reduced lock-length and with lock-slope. The dashed line is the identity line.

where the limits of integration are $T_1 = L_h$ and $T_2 = L_b$, in order to focus on the body, the region that has been found mostly affected by the variation of the initial conditions. The validity of the use of Φ_m as an indicator of the entrainment capacity is supported by the analysis of its relation with the Richardson number Ri (Zordan et al., under review, b). The relation between water entrainment and bulk Richardson number is well known in literature and numerous empirical fits to the experimental data have been proposed since the early work of Parker et al. (1987) and supported by more recent contributions (Stagnaro and Pittaluga, 2014). Therefore, it is here proposed to use this quantity as a surrogate for water entrainment capacity since it benefits from the instantaneous measurements of shear stress and therefore account for the unsteady behaviour of the gravity currents. In Figure 9, the potential water entrainments for gravity currents performed on an inclined and correspondent tests with reduced initial volume of release are compared. The tests S4L4 detach from the identity line, thus a greater water entrainment is expected for the case with the inclined bed with respect to the horizontal bottom.

4.3 Bottom erosion capacity

Similarly to the interfacial water entrainment capacity, the bottom entrainment capacity, that can also be called the erosion capacity is here computed.

This new quantity is computed as:

$$\Phi_b = \int_{T_1}^{T_2} \tau_b(t)dt/t^* \tag{7}$$

where the limit T_i are $T_1 = 0$, $T_2 = L_b$. In Zordan et al. (under review, a) this quantity proved to be a surrogate of the entrainment capacity of a gravity current produced over a mobile bed.
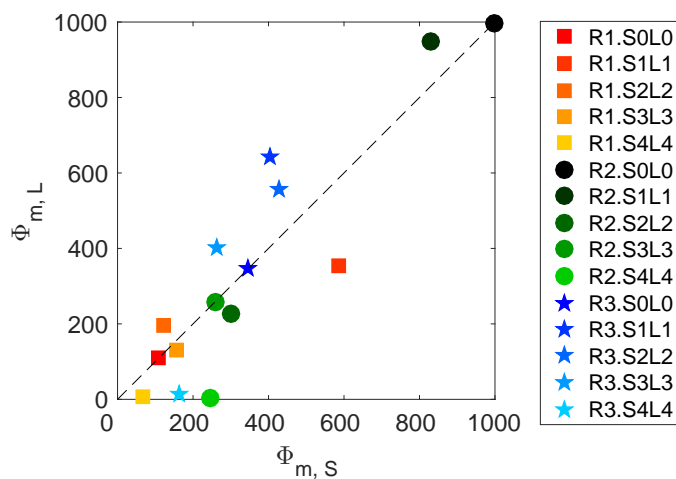
Figure 9. Comparison of Φ_m, a surrogate for the entrainment capacity of the mixing region, between tests with lock-slope (S_i) and correspondent tests on horizontal bottom (L_i). The dashed line is the identity line.
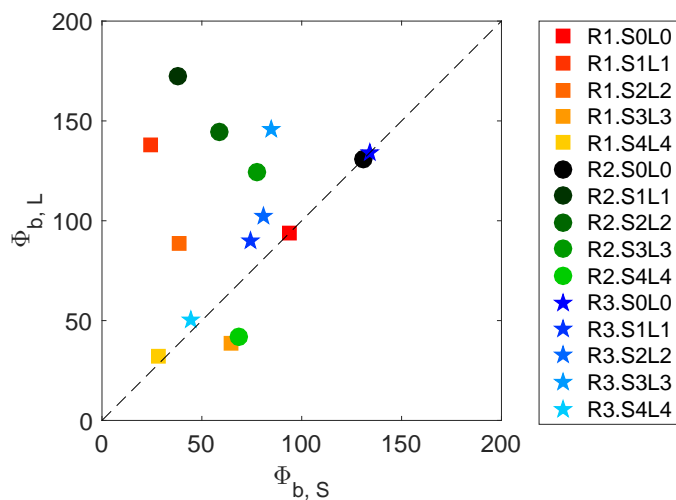
Figure 10. Comparison of the bottom erosion capacity Φ_b between tests with lock-slope (S_i) and correspondent tests on horizontal bottom (L_i). The dashed line is the identity line.
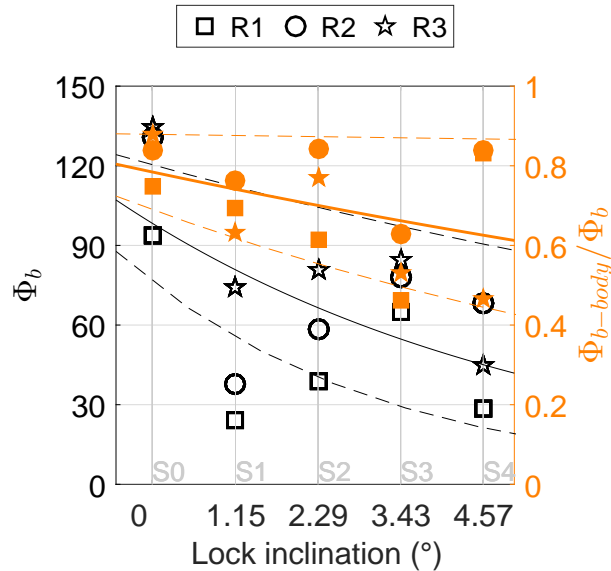
Figure 11. Potential erosion capacity for gravity currents (left axis) developed with different lock-inclinations and rate of potential bottom erosion due to the body of the gravity current on the total bottom erosion capacity, $\Phi_{b-body}/\Phi b$, (right axis). The exponential fitting lines are reported in order to give evidence of the general trend, together with the 85% confidence intervals (dashed lines).

The bottom erosion capacity is compared for gravity currents performed with the lock-slope and correspondent tests on a horizontal bottom. Generally L_i tests show a higher erosion capacity with respect to their analogous S_i. The presence of an extra gravitational force is proved not to play a role in enhancing bottom erosion which is contrarily reduced. This is probably a consequence of the decrease in streamwise velocity which results from the dilution of the gravity current. But, on the other

5 hand, ambient water entrainment causes the expansion of the body region. Longer bodies keep eroding material longer and the erosion potential attributed to this part is therefore increasing. The potential bottom erosion, i.e. the quantity Φ_b in Figure 11, show a tendency to decrease with increasing slope. The role of the body in the total erosion capacity is computed as the ratio Φ_{b-body}/Φ_b (Figure 11) whose limits of integration of Φ_{b-body} are $T_1 = L_h$ and $T_2 = L_b$. The contribution that is ascribed to the body has a similar development as the total erosion capacity. This enforce the hypothesis that the body is determinant in

10 the entrainment capacity of a gravity current. Figure 11 highlights that the importance of the body in the total erosion capacity becomes proportionally higher for tests S4 (the trend lines in Figure 11 deviates more in this configuration). Higher water entrainment was proved in Section 4.2 for this latter case, which was therefore subjected to an expansion of the body region. An influence of the upper surface on the dynamics of the lower bottom boundary is therefore hypothesized. The interaction between the upper layer and the bottom was already pointed out by the numerical investigation of Cantero et al. (2008) and

15 experimental evidences were reported in Zordan et al. (under review, b). In this latter the vorticity was analysed showing that residual negative vorticity expands from the upper layer through the bottom with progressively lower intensity.

5 Conclusion

In this paper the effect of incremental gravitational forces is tested by reproducing experimentally gravity currents of different initial densities with the presence of an inclines lock. Corresponding tests on a horizontal bottom are performed as well in order to have the reference cases with reduced volume. The range of lock-slopes tested varies from horizontal bed to $S < 8\%$ (which

5 correspond to an inclination of the lock $\alpha < 5°$). Gravitational force is the main driving force which directly depends on slope (Khavasi et al., 2012). These compete with the entrainment that takes place due to higher shear stress at the upper interface and tend to dilute the current. Thus if on one hand gravitational acceleration drives for a faster gravity current, on the other hand water entrainment at the upper interface dilute the fluid of the current which is consequently slowed down and it expands due to incorporation of the ambient fluid. The configurations S4-L4, corresponding to the steepest lock-slope and the shortest lock-

10 length, respectively, exhibit the highest deviations between tests with lock-slopes with respect to correspondent tests on the horizontal bed. S4 tests showed a longer body, owing to entrainment of the ambient fluid. The body is fast, likely accelerated due to gravitational effects. Bottom erosion capacity generally results reduced by the presence of the extra gravitational forces most probably due to lower streamwise velocities which followed gravity currents dilution. The limit case of tests S4, with a lock-slope of $S = 8\%$, are probably facing the transient condition as described by previous literature (Britter and Linden

15 (1980), Beghin et al. (1981), Parker et al. (1987), Maxworthy and Nokes (2007), Maxworthy (2010)). The limit given by the experimental set up did not allow to go for steeper lock-slopes, cases for which therefore further investigation should be undertaken. The present study analyses changing initial conditions which trigger gravity currents that are commonly observed in nature.

Competing interests. The authors have no conflict of interest to declare.

20 *Acknowledgements.* This research was funded by the European project SEDITRANS funded by Marie Curie Actions, FP7-PEOPLE-2013-ITN-607394 (Multi partner - Initial Training Networks).

References

Ancey, C.: Gravity flow on steep slope, vol. Buoyancy Driven Flows, Cambridge University Press New York, 2012.

Baas, J. H., McCaffrey, W. D., Haughton, P. D., and Choux, C.: Coupling between suspended sediment distribution and turbulence structure in a laboratory turbidity current, Journal of Geophysical Research: Oceans, 110, 2005.

5 Beghin, P., Hopfinger, E., and Britter, R.: Gravitational convection from instantaneous sources on inclined boundaries, Journal of Fluid Mechanics, 107, 407–422, 1981.

Britter, R. and Linden, P.: The motion of the front of a gravity current travelling down an incline, Journal of Fluid Mechanics, 99, 531–543, 1980.

Cantero, M. I., Balachandar, S., García, M. H., and Bock, D.: Turbulent structures in planar gravity currents and their influence on the flow 10 dynamics, Journal of Geophysical Research: Oceans, 113, 2008.

Chassaing, P.: Mécanique des fluides, Cepadues éditions, 2010.

Csanady, G. T.: Turbulent interface layers, Journal of Geophysical Research: Oceans, 83, 2329–2342, 1978.

Ellison, T. and Turner, J.: Turbulent entrainment in stratified flows, Journal of Fluid Mechanics, 6, 423–448, 1959.

Fer, I., Lemmin, U., and Thorpe, S.: Winter cascading of cold water in Lake Geneva, Journal of Geophysical Research: Oceans, 107, 2002.

15 Ferreira, R. M.: The von Kármán constant for flows over rough mobile beds. Lessons learned from dimensional analysis and similarity, Advances in Water Resources, 81, 19–32, 2015.

Ferreira, R. M., Franca, M. J., Leal, J. G., and Cardoso, A. H.: Flow over rough mobile beds: Friction factor and vertical distribution of the longitudinal mean velocity, Water Resources Research, 48, 2012.

Franca, M. and Lemmin, U.: Eliminating velocity aliasing in acoustic Doppler velocity profiler data, Measurement Science and Technology, 20 17, 313, 2006.

Goring, D. G. and Nikora, V. I.: Despiking acoustic Doppler velocimeter data, Journal of Hydraulic Engineering, 128, 117–126, 2002.

Huppert, H. E.: Gravity currents: a personal perspective, Journal of Fluid Mechanics, 554, 299–322, 2006.

Hurther, D. and Lemmin, U.: A correction method for turbulence measurements with a 3D acoustic Doppler velocity profiler, Journal of Atmospheric and Oceanic Technology, 18, 446–458, 2001.

25 Khavasi, E., Afshin, H., and Firoozabadi, B.: Effect of selected parameters on the depositional behaviour of turbidity currents, Journal of Hydraulic Research, 50, 60–69, 2012.

Kneller, B. and Buckee, C.: The structure and fluid mechanics of turbidity currents: a review of some recent studies and their geological implications, Sedimentology, 47, 62–94, 2000.

Lemmin, U. and Rolland, T.: Acoustic velocity profiler for laboratory and field studies, Journal of Hydraulic Engineering, 123, 1089–1098, 30 1997.

Lofquist, K.: Flow and stress near an interface between stratified liquids, The Physics of Fluids, 3, 158–175, 1960.

Maxworthy, T.: Experiments on gravity currents propagating down slopes. Part 2. The evolution of a fixed volume of fluid released from closed locks into a long, open channel, Journal of Fluid Mechanics, 647, 27–51, 2010.

Maxworthy, T. and Nokes, R.: Experiments on gravity currents propagating down slopes. Part 1. The release of a fixed volume of heavy fluid 35 from an enclosed lock into an open channel, Journal of Fluid Mechanics, 584, 433–453, 2007.

Ninto, Y. and Garcia, M.: Experiments on particle—turbulence interactions in the near–wall region of an open channel flow: implications for sediment transport, Journal of Fluid Mechanics, 326, 285–319, 1996.

Nogueira, H. I., Adduce, C., Alves, E., and Franca, M. J.: Dynamics of the head of gravity currents, Environmental Fluid Mechanics, 14, 519–540, 2014.

Palmieri, A., Shah, F., and Dinar, A.: Economics of reservoir sedimentation and sustainable management of dams, Journal of Environmental Management, 61, 149–163, 2001.

5 Parker, G., Garcia, M., Fukushima, Y., and Yu, W.: Experiments on turbidity currents over an erodible bed, Journal of Hydraulic Research, 25, 123–147, 1987.

Salim, S., Pattiaratchi, C., Tinoco, R., Coco, G., Hetzel, Y., Wijeratne, S., and Jayaratne, R.: The influence of turbulent bursting on sediment resuspension under unidirectional currents, Earth Surface Dynamics, 5, 399, 2017.

Schleiss, A. J., Franca, M. J., Juez, C., and De Cesare, G.: Reservoir sedimentation, Journal of Hydraulic Research, 54, 595–614, 2016.

10 Simpson, J. E.: Effects of the lower boundary on the head of a gravity current, Journal of Fluid Mechanics, 53, 759–768, 1972.

Simpson, J. E.: Gravity currents in the environment and in the laboratory: Chichester, 1987.

Simpson, J. E.: Gravity currents: In the environment and the laboratory, Cambridge university press, 1997.

Stagnaro, M. and Pittaluga, M. B.: Velocity and concentration profiles of saline and turbidity currents flowing in a straight channel under quasi-uniform conditions, Earth Surface Dynamics, 2, 167, 2014.

15 Turner, J. S.: Buoyancy effects in fluids, Cambridge University Press, 1973.

Ungarish, M.: An introduction to gravity currents and intrusions, CRC Press, 2009.

Zordan, J., Juez, C., Schleiss, A. J., and Franca, M. J.: Erosion and deposition of sediment by saline gravity currents, Sedimentology, under review, a.

Zordan, J., Schleiss, A. J., and Franca, M. J.: Structure of a dense release produced by varying initial conditions, Environmental Fluid
20 Mechanics, under review, b.